Substrate-Induced Fit of the ATP Binding Site of Cytidine Monophosphate Kinase from *Escherichia coli*: Time-Resolved Fluorescence of 3′-Anthraniloyl-2′-deoxy-ADP and Molecular Modeling†

Inès M. Li de la Sierra,[#,‡] Jacques Gallay,*[,§] Michel Vincent,[§] Thomas Bertrand,[⊥] Pierre Briozzo,[||] Octavian Bârzu,[#] and Anne-Marie Gilles[#]

LURE Bâtiment 209D, UMR 130 CNRS Université Paris-Sud, 91898 Orsay Cedex, France, Laboratoire de Chimie Structurale des Macromolécules, URA 2185 CNRS, Institut Pasteur, 75724 Paris Cedex 15, France, Laboratoire de Chimie Biologique, Institut National Agronomique, Paris-Grignon 78850 Thiverval-Grignon, France, and Laboratoire d'Enzymologie et de Biochimie Structurale, UPR CNRS 9063, 91198 Gif-sur-Yvette Cedex, France

Received July 5, 2000; Revised Manuscript Received October 17, 2000

ABSTRACT: The conformation and dynamics of the ATP binding site of cytidine monophosphate kinase from *Escherichia coli* ($CMPK_{coli}$), which catalyzes specifically the phosphate exchange between ATP and CMP, was studied using the fluorescence properties of 3′-anthraniloyl-2′-deoxy-ADP, a specific ligand of the enzyme. The spectroscopic properties of the bound fluorescent nucleotide change strongly with respect to those in aqueous solution. These changes (red shift of the absorption and excitation spectra, large increase of the excited state lifetime) are compared to those observed in different solvents. These data, as well as acrylamide quenching experiments, suggest that the anthraniloyl moiety is protected from the aqueous solvent upon binding to the ATP binding site, irrespective of the presence of CMP or CDP. The protein-bound ADP analogue exhibits a restricted fast subnanosecond rotational motion, completely blocked by CMP binding. The energy-minimized models of $CMPK_{coli}$ complexed with 3′-anthraniloyl-2′-deoxy-ADP using the crystal structures of the ligand-free protein and of its complex with CDP (PDB codes 1cke and 2cmk, respectively) were compared to the crystal structure of UMP/CMP kinase from *Dictyostelium discoideum* complexed with substrates (PDB code 3ukd). The key residues for ATP/ADP binding to $CMPK_{coli}$ were identified as R157 and I209, their side chains sandwiching the adenine ring. Moreover, the residues involved in the fixation of the phosphate groups are conserved in both proteins. In the model, the accessibility of the fluorescent ring to the solvent should be substantial if the LID conformation remained unchanged, by contrast to the fluorescence data. These results provide the first experimental arguments about an ATP-mediated induced-fit of the LID in $CMPK_{coli}$ modulated by CMP, leading to a closed conformation of the active site, protected from water.

CMPKs,[1] like other nucleoside monophosphate kinases, are key enzymes in the metabolism of nucleotides including synthesis of RNA and DNA molecules (*1, 2*). $CMPK_{coli}$ is a monomeric protein containing 227 residues. It plays an important role since it catalyses specifically the transfer of phosphate from ATP to CMP. UMP is an extremely poor substrate for this protein. To synthesize UDP, *Escherichia coli* possesses a separated UMP kinase specific for UMP (*3*). This is in contrast to UMP/CMP kinases from eukaryotes which can phosphorylate both CMP and UMP with the same efficiency. A second feature of $CMPK_{coli}$ is its ability to phosphorylate dCMP, which is a poor substrate for eukaryotic UMP/CMP kinases. Third, binding of CMP enhances the affinity of $CMPK_{coli}$ for ATP or ADP, a property never described in other NMPKs (*4*). Together with the presence of a long insertion in the NMP binding domain (see below), this allows consideration of $CMPK_{coli}$ as an original NMP kinase, the only CMPK with a known three-dimensional structure (*5*).

The particular function of the $CMPK_{coli}$ in the nucleotide metabolic pathways in the bacteria aroused investigations

† I.M.L.S. wishes to acknowledge financial support from the laboratory during the course of this work. M.V. acknowledges the Institut National de la Santé et de la Recherche Médicale for its continual financial support. This work was supported also by grants from Institut Pasteur, from the Centre National de la Recherche Scientifique (URA 2185) and from the Ministère de l'Education Nationale, de la Recherche et de la Technologie (contract no. 88T0823).

* Corresponding author at LURE Bâtiment 209D, Université Paris-Sud, BP 34, 91898 ORSAY Cedex, France. Fax/telephone: 33 1 64 46 80 82; e-mail: gallay@lure.u-psud.fr.

[#] Institut Pasteur.

[‡] Present address: Laboratoire d'Enzymologie et de Biochimie Structurale.

[§] Université Paris-Sud.

[⊥] Laboratoire d'Enzymologie et de Biochimie Structurale.

[||] Institut National Agronomique.

[1] Abbreviations: AMPK, adenylate kinase; Ant-dADP, 3′-anthraniloyl-2′-deoxy-ADP; Ant-Me, methyl anthranilate; CMP, cytidine 5′-monophosphate; dCMP, 2′-deoxycytidine 5′-monophosphate; CDP, cytidine 5′-diphosphate; CMPK, cytidine monophosphate kinase; $CMPK_{coli}$, cytidine monophosphate kinase from *E. coli*; MEM, maximum entropy method; NMP_{bind}, nucleoside monophosphate binding site; NMPK, nucleoside monophosphate kinase; TMPK, thymidine monophosphate kinase; UMP, uridine 5′-monophosphate; $UMPK_{dict}$, UMP/CMP kinase from *Dictyostelium discoideum.*

10.1021/bi0015360 CCC: $19.00
Published on Web 12/02/2000

of its structure and reactivity. The crystal structures of the protein alone and complexed with CDP (*5*) exhibit strong similarities with those of other NMPKs, characterized by a central five-stranded parallel β-sheet connected by α-helices (*6*). The $CMPK_{coli}$ enzyme differs however from the others by the presence of one insertion of 40 residues inside the NMP_{bind}, leading to a particular topology with two subdomains: a first one comprising three antiparallel β-strands and a second one including two α-helices (*5*). The NMP_{bind} insert undergoes a large rearrangement upon CDP binding, leading to a closed conformation protecting CDP from the solvent. The region covering the ATP binding site (namely, the LID) seemed to undergo also a conformational change upon CDP binding (*5*), leading to a more "opened" structure. CMP and dCMP provoke a similar structural change of the LID (Bertrand and Briozzo, unpublished observations), which could facilitate the phosphate donor binding. In agreement with these observations, the presence of the phosphate acceptor enhances the respective affinities of ADP, Ant-dADP, and Ant-dATP by 1 order of magnitude (*4*). We expect that binding of ATP provokes a further conformational change of the LID, to protect the transferred phosphate from water. Substrate-induced movements have been experimentally evidenced for AMPKs (*7*−*10*) and more recently for TMPK (*11*). Nevertheless, this expected effect of ATP binding on the structure and flexibility of the $CMPK_{coli}$ LID region is still unknown, the crystallization of the binary or ternary complexes of the protein with its substrates remaining unsuccessful.

To get information on the structural change of the LID domain upon binding of ATP and analogues to this protein, we labeled the ATP binding site with a fluorescent derivative of dADP (Ant-dADP), which is a high affinity ligand of the *E. coli* enzyme (*4*). The anthraniloyl probes have been introduced initially to label the nucleotide-binding site of cyclic nucleotide phosphodiesterase (*12*). They present the advantages of possessing a small extra size as compared to the entire nucleotide and to provide a strong fluorescence signal when bound to proteins (*13*). The fluorescence decays of the bound probes are usually characterized by long lifetime values of around 8−10 ns, a time-window that allows separating quite easily its internal rotational motion from the Brownian rotation of the entire protein (*14*). Ant-dADP displays a dissociation constant for the $CMPK_{coli}$ in the micromolar range of concentration. It is removed competitively by ATP (*4*). Binding of the fluorescent nucleotide to the protein enhanced the fluorescence intensity by a factor 3−4 while the emission spectrum was slightly blue-shifted (*4*). This strong binding and this large fluorescence enhancement allowed us to use Ant-dADP to probe the dynamic properties of the ATP binding site and to evaluate the influence of CMP, dCMP, and CDP binding on these properties. The present results evidence the inaccessibility of the anthraniloyl ring to the aqueous solvent, either in the presence or in the absence of CMP, CDP, or dCMP. Molecular modeling of a complex of the protein with Ant-dADP using the protein crystal structure shows, by contrast, that the anthraniloyl moiety should be highly accessible to water if no conformational change occurred. This suggests that the expected ATP-induced conformational change of the LID really occurs, either in the presence or in the absence of the phosphate acceptor. Moreover, CMP binding further alters the conformation and dynamics of the LID, leading to a complete immobilization of the fluorophore in the ternary complex. By contrast, dCMP and CDP display weaker effects. These findings offer a molecular basis for the understanding of the specificity of catalysis of this protein and suggest an ordered mechanism of the enzymatic reaction.

MATERIALS AND METHODS

Chemicals. Ant-dADP was prepared according to published procedures (*4*, *15*). All chemicals were of the highest grade commercially available.

Protein Preparation. $CMPK_{coli}$ was purified as previously described, and its activity was determined using a coupled spectrophotometric assay (*4*, *16*).

Steady-State and Time-Resolved Fluorescence Measurements. Steady-state fluorescence excitation spectra were recorded between 250 and 400 nm (bandwidth 2 nm) on a SLM 8000 spectrofluorometer. Fluorescence intensity and anisotropy decays were obtained by the time-correlated single photon counting technique from the polarized components $I_{vv}(t)$ and $I_{vh}(t)$ on the experimental setup installed on the SB_1 window of the synchrotron radiation machine Super-ACO (Anneau de Collision d'Orsay) (*17*). The excitation and the emission wavelengths were selected, respectively, by a double monochromator (Jobin Yvon UV-DH10, bandwidth 4 nm) and by a single monochromator (Jobin Yvon UV-H10, bandwidth 8 nm). A MCP-PMT Hamamatsu detector (model R3809U-02) was used. Time resolution was ~20 ps, and the data were stored in 2048 channels. Automatic sampling cycles including 30 s accumulation time for the instrument response function and 90 s acquisition time for each polarized component were carried out until a total number of 2−4 10^6 counts was reached in the fluorescence intensity decay.

Data Analysis of Fluorescence Intensity and Anisotropy Decays. Analyses of fluorescence intensity decays as sums of exponentials were performed by the maximum entropy method (MEM) (*18*, *19*). Analysis of the polarized fluorescence decays were performed by the one-dimensional model of the anisotropy, in which each lifetime τ_i is coupled to any rotational correlation time θ_i (*18*, *20*). Sets of 150 and 100 independent variables, equally spaced in log scale, were used for the fluorescence intensity and anisotropy decays, respectively.

A two-dimensional $\Gamma(\tau, \theta)$ analysis, essential to describe the coupling between lifetimes and rotational correlation times, was also used (*18*, *21*−*25*). This analysis starts with an initial model of the $\Gamma(\tau, \theta)$ distribution as a "flat" map where all the (τ, θ) are equiprobable. It allows the delineation of the (τ, θ) associations with the less possible a priori hypotheses. It is nevertheless intrinsically limited, since the polarized fluorescence decays involve in their expressions a time constant that is a harmonic mean κ_i between τ_i and θ_i: $1/\kappa_i = 1/\tau_i + 1/\theta_i$ where τ_i and θ_i can be exchanged without any modification in the κ_i value, leading to construction of iso-kappa curves. These iso-kappa contours are visualized on the two-dimensional (τ, θ) maps by dotted lines. This degeneracy is especially troublesome when short lifetimes are coupled to long correlation times and conversely as shown by simulations (*18*). Calculations in double precision allows one to overcome this problem for a large part.

For fluorescence intensity and anisotropy decay analysis (with the one-dimensional model), computations were performed on a DEC Vax station 4000/90. Two-dimensional analyses were carried out on a DEC alpha computer Vax 7620 with a set of 1600 independent variables (40 τ and 40 θ equally spaced in log scale). The programs including the MEMSYS 5 subroutines (MEDC Ltd., Cambridge U. K.) were written in double precision FORTRAN 77.

Molecular Modeling of the CMPK$_{coli}$ Complexes with Ant-dADP. Models of the three-dimensional structure of the complexes of CMPK_{coli} with Ant-dADP were constructed using the X-ray crystal structures of the ligand-free CMPK$_{coli}$ (PDB code 1cke) or of its complex with CDP (PDB code 2cmk) (*5*) and that of the UMPK$_{dict}$/ADP/CMP/AlF_3 complex (PDB code 3ukd) (*26*), both proteins sharing strong structural homologies. The same procedure as that described for the modeling of the ternary trypsin/chymotrypsin/PSTI-V complex from pea seeds was used (*27*). In a first step, the structures of CMPK$_{coli}$ and of UMPK$_{dict}$ were superimposed using only the core of the five-stranded β-sheet, with the procedure implemented in the O program (*28*). Then, the Ant-dADP molecule was placed in the CMPK$_{coli}$ structure in a similar way as the ADP molecule in the UMPK$_{dict}$/ADP/CMP complex. Two structural characteristics were imposed: the β-phosphate and the adenine moiety positions. The β-phosphate of the Ant-dADP was placed at the S1 site of the ligand-free CMPK$_{coli}$ structure (*5*), since a sulfate ion always occupies this position when the NMPKs crystallize in the absence of phosphate donor ligand and in the presence of ammonium sulfate (*29*−*31*). The β-phosphate is present at this site in the crystal structures of NMPKs complexed with ATP analogues (*8*). The adenine moiety was oriented along with the R157 side chain, a strongly conserved residue, as observed in the structures of other complexes of NMPKs with phosphate donor analogues (*32*, *33*). The same procedure was performed to model the CMPK$_{coli}$/CDP/Ant-dADP complex beginning from the X-ray structure of the CMPK$_{coli}$/CDP complex (*5*) and the UMPK$_{dict}$/ADP/CMP/AlF_3 complex. The two models were finally energy-minimized to eliminate improper atomic overlaps and poor geometry, with the procedure implemented in XPLOR (*34*).

RESULTS

Spectroscopic Properties of Ant-dADP and of Ant-Me in Water and in Organic Solvents. The environment strongly affects the spectroscopic properties of the anthraniloyl chromophore. The lowest energy absorption band of Ant-Me displays a maximum at 327 nm in water. It shifts to 339−340 nm in less polar protic solvents such as MeOH and EtOH (not shown) and further to 342−343 nm in aprotic polar solvents such as DMSO and DMF, while the absorption spectra in the apolar solvent cyclohexane displays a maximum at 333 nm (not shown).

The fluorescence intensity decays of both Ant-Me and Ant-dADP in water are described by one major excited-state lifetime of 1.9 ns and by a minor subnanosecond one (0.2−0.5 ns) (Figure 1, panels A and B and Table 1). The identity of both decays rules out any contribution of stacking interactions between the anthraniloyl and the adenine rings, which were formerly assumed to occur in water to explain the short excited-state lifetime of the fluorescent nucleotide

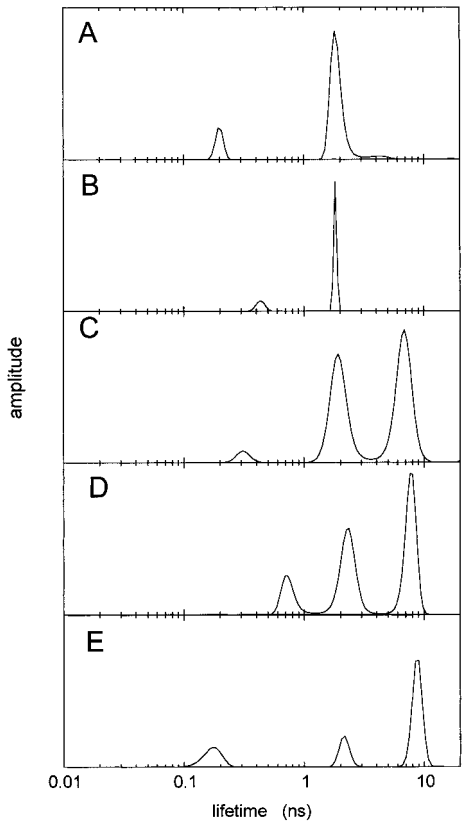

FIGURE 1: Excited-state lifetime distribution of the fluorescence intensity decays of (A) Ant-dADP 4 μM in water; (B) Ant-Me 4 μM in water; (C) Ant-dADP (3.8 μM) in the presence of CMPK$_{coli}$ (10.8 μM) without CMP; (D) Ant-dADP (3.8 μM) in the presence of CMPK$_{coli}$ (10.8 μM) with CDP 1 mM; and (E) Ant-dADP (3.8 μM) in the presence of CMPK$_{coli}$ (10.8 μM) with CMP 1 mM. MEM analysis as a sum of exponentials was performed on the fluorescence intensity $T(t)$ reconstructed from the parallel and perpendicular polarized components $I_{vv}(t)$ and $I_{vh}(t)$ as described in the legend of Table 1. Excitation wavelength: 340 nm; emission wavelength: 425 nm for the anthraniloyl derivatives in buffer and 410 nm in the presence of CMPK$_{coli}$.

(*35*). The fluorescence intensity decay in D_2O is also multiexponential and evidences a characteristic isotopic effect on the major long lifetime of around 25% (Table 1). Deuterium isotope effects on fluorescence have been interpreted as evidence for excited-state proton-transfer reactions (*36*). These observations suggest therefore a mechanism of quenching by water involving a proton exchange between the anthraniloyl excited-state and the aqueous solvent. In agreement with this conclusion, the fluorescence intensity decays in organic polar solvents are monoexponential and display much longer excited-state lifetime values than in water (Table 1). The largest values are observed in the strongest aprotic polar solvents DMF and DMSO.

Spectroscopic Characteristics of Ant-dADP Bound to CMPK$_{coli}$. The fluorescence intensity of Ant-dADP is increased ∼4 times upon binding to CMPK$_{coli}$. A blue shift of the maximum of emission of ∼10 nm (*4*) and a red shift of the maximum of absorption (not shown) and of the excitation spectra of ∼10 nm are observed (Figure 2). The fluorescence intensity increase upon binding of the inhibitor to the protein is completely accounted for by the appearance of a long excited-state lifetime of 6.8 ns (Figure 1, panel C), of the order of the values measured in nonaqueous polar solvents. Two shorter lifetimes, with values similar to those

Table 1: Fluorescence Intensity Decay Parameters of Ant-dADP and of Ant-Me in Different Solvents[a]

solvent	fluorescent probe	τ_1 (ns)[b] C_1[b]	τ_2 (ns) C_2	τ_3 (ns) C_3
water	Ant-dADP	0.2	1.9	10.5
		0.13	*0.86*	*0.01*
methanol	Ant-dADP		3.2	7.3
			0.01	*0.99*
ethanol	Ant-dADP		1.36	7.52
			0.01	*0.99*
water	Ant-Me	0.4	1.9	
		0.23	*0.77*	
D_2O	Ant-Me	0.6	2.4	
		0.20	*0.80*	
methanol	Ant-Me		1.9	7.4
			0.01	*0.99*
ethanol	Ant-Me			7.6
				1
THF	Ant-Me			7.6
				1
DMF	Ant-Me			8.1
				1
DMSO	Ant-Me			9.0
				1
cyclohexane	Ant-Me	0.1		4.9
		0.02		*0.98*

[a] MEM analysis was performed on the fluorescence intensity $T(t)$ reconstructed from the parallel and perpendicular polarized components $I_{vv}(t)$ and $I_{vh}(t)$ such as $T(t) = I_{vv}(t) + 2\beta_{corr}I_{vh}(t) = \int_0^\infty \alpha(\tau)\exp(-t/\tau)d\tau$. τ is the excited state lifetime, $\alpha(\tau)$ is its amplitude, and β_{corr} is the correction factor accounting for the difference in transmission of the vertical and horizontal components (58). Experiments were performed at 20 °C. [b] τ_i and C_i (italicized numbers) are, respectively, the values of the center and of the normalized amplitude of each lifetime peak.

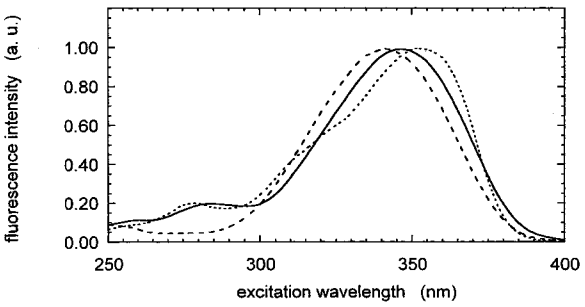

FIGURE 2: Steady-state fluorescence excitation spectra of Ant-dADP. Emission wavelength: 420 nm; broken line: Ant-dADP in water at room temperature; plain line: Ant-dADP in the presence of $CMPK_{coli}$ at room temperature; dotted line: Ant-dADP in ethanol at 173 K.

Table 2: Fluorescence Intensity Decay Parameters of Ant-dADP Unbound and Complexed with $CMPK_{coli}$[a]

sample	τ_1 (ns)[b] C_1[b] I_1[c]	τ_2 (ns) C_2 I_2	τ_3 (ns) C_3 I_3	$\langle\tau\rangle$ (ns)[d]
Ant-dADP	0.22	2.0	10.4	1.83
	0.13	*0.86*	*0.01*	
	0.01	*0.94*	*0.05*	
$CMPK_{coli}$/Ant-dADP	0.31	2.0	6.8	4.41
no CMP	*0.04*	*0.44*	*0.52*	
	<0.01	*0.20*	*0.80*	
$CMPK_{coli}$/Ant-dADP	0.17	2.2	8.7	5.74
1 mM CMP	*0.21*	*0.18*	*0.61*	
	<0.01	*0.07*	*0.93*	
$CMPK_{coli}$/Ant-dADP	0.82	2.4	7.3	4.37
1 mM dCMP	*0.15*	*0.40*	*0.45*	
	0.03	*0.22*	*0.75*	
$CMPK_{coli}$/Ant-dADP	0.74	2.3	7.7	4.58
1 mM CDP	*0.15*	*0.38*	*0.47*	
	0.02	*0.19*	*0.79*	

[a] Ant-dADP concentration: 3−3.8 μM; $CMPK_{coli}$ concentration: 10.8 μM; excitation wavelength: 325 nm; emission wavelength: 425 nm for free Ant-dADP and 410 nm in the presence of $CMPK_{coli}$; temperature: 20 °C. [b] τ_i and C_i (italicized numbers) are, respectively, the values of the center and of the normalized amplitude of each lifetime peak. [c] The partial intensities I_i (italicized numbers) of each lifetime species were calculated as $I_i = (C_i\tau_i/\langle\tau\rangle)$. [d] The mean excited-state lifetime was calculated according to $\langle\tau\rangle = \sum_i C_i\tau_i$.

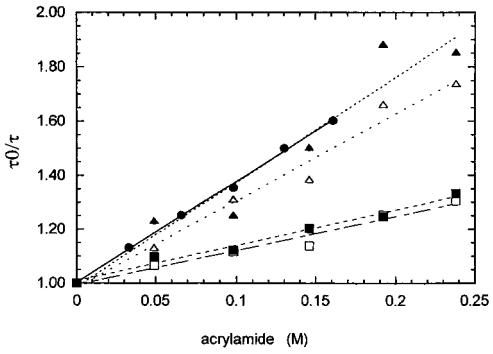

FIGURE 3: Stern−Volmer plots of time-resolved acrylamide quenching of Ant-dADP fluorescence in water (3.8 mM) and in the presence of $CMPK_{coli}$ (10.8 μM) (●) τ_2 of Ant-dADP in water (regression coefficient: 0.999); (△) τ_2 of Ant-dADP in the presence of $CMPK_{coli}$ without CMP (regression coefficient: 0.989); (▲) τ_2 in the presence of $CMPK_{coli}$ with CMP 1 mM (regression coefficient: 0.964); (□) τ_3 in the presence of $CMPK_{coli}$ without CMP (regression coefficient:0.983); (■) τ_3 in the presence of $CMPK_{coli}$ with CMP 1 mM (regression coefficient: 0991).

of Ant-dADP and of Ant-Me in water, are also present. CMP binding to the *E. coli* enzyme provokes an increase by 28% of the long excited-state lifetime τ_3 value (up to 8.7 ns) and of its amplitude (Figure 1, panel E, and Table 2). CDP (Figure 1, panel D) and dCMP provoke smaller increases of the lifetime values by around 13 and 7%, respectively, and weak amplitude changes (Table 2). No fluorescence resonance energy transfer between the Trp residue (W31) and the anthraniloyl ring can be evidenced on the fluorescence excitation spectrum, the weak extra band observed at 285 nm in the $CMPK_{coli}$/Ant-dADP complex being also present for Ant-dADP in ethanol at low temperature (Figure 2). It seems to be an intrinsic spectroscopic property of the probe interacting with the solvent.

Accessibility to the Solvent of the Anthraniloyl Group in the $CMPK_{coli}$/Ant-dADP Complexes. We have estimated the degree of exposure to the aqueous solvent of the anthraniloyl group of Ant-dADP bound to $CMPK_{coli}$ by time-resolved fluorescence quenching experiments using acrylamide, a water-soluble molecule (*37*, *38*). These measurements were performed on Ant-dADP free and bound to $CMPK_{coli}$ in the presence and in the absence of 1 mM CMP. The Stern−Volmer plots obtained with the intermediate lifetime ($\tau_2 \approx$ 2 ns) and with the long one ($\tau_3 = 6.8$ ns without CMP and 8.7 ns in the presence of 1 mM CMP) are linear (Figure 3). The Stern−Volmer constant K_{sv} and the calculated bimolecular quenching constant k_q, corresponding to τ_2, display respective values almost identical to that of free Ant-dADP in water. This strongly suggests that this lifetime population is due to the free inhibitor. By contrast, the K_{sv} values, corresponding to the long lifetime population, are ~3 times smaller, and the calculated bimolecular quenching constant

Table 3: Acrylamide Quenching Constants for Ant-dADP Unbound and Complexed with $CMPK_{coli}$[a]

sample	lifetime species	(ns)	K_{sv} (M^{-1})	$k_q \times 10^9$ (M^{-1} s^{-1})
Ant-dADP	τ_2	2.1	3.7	1.8
$CMPK_{coli}$/Ant-dADP	τ_2	2.0	3.2	1.6
	τ_3	6.8	1.3	0.19
$CMPK_{coli}$/CMP/Ant-dADP	τ_2	2.1	3.9	1.9
	τ_3	8.8	1.3	0.15

[a] Temperature 20 °C.

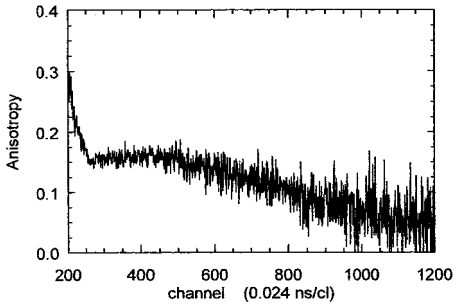

FIGURE 4: Experimental fluorescence anisotropy decay $A(t)$ of Ant-dADP (3.8 μM) with $CMPK_{coli}$ (10.8 μM) in the presence of 1 mM CMP. $A(t) = [I_{vv}(t) - \beta_{corr}I_{vh}(t)/I_{vv}(t) + 2\beta_{corr}I_{vh}(t)]$. β_{corr} is the correction factor defined in the legend of Table 1.

k_q values are 1 order of magnitude smaller than the respective values for the free inhibitor (Table 3). Estimation of the solvent accessibility from this value according to Johnson and Yguerabide (*39*) leads to a surface area of around 5% with respect to that of free Ant-dADP. The bound Ant-dADP is therefore almost fully shielded from contact with the solvent in the $CMPK_{coli}$ both in the absence and in the presence of CMP.

Rotational Dynamics of Ant-dADP Free and Bound to $CMPK_{coli}$. The experimental fluorescence anisotropy decay curve of the probe bound to the protein exhibits an irregular pattern with a fast decrease followed by a slope inversion, a slow increase to a maximum and then a slow decay to zero (Figure 4). The fluorescence anisotropy decay is therefore nonexponential and cannot be adequately described by the classical one-dimensional model associating each lifetime with each rotational correlation time, resulting in poor fitting parameters: high chi-square value and nonrandom pattern of the deviation function (not shown). Acrylamide quenching experiments suggested that the 2 ns lifetime component likely characterizes the free fluorescent nucleotide, whereas the long lifetime is due to the bound nucleotide. Therefore, fast rotations are likely associated more specifically with the short lifetimes, and conversely, slow Brownian rotation is associated specifically to the longest lifetime.

Thus, we performed a two-dimensional (τ, θ) analysis of the polarized fluorescence intensity decays. This analysis starts without any a priori association between lifetimes and correlation times and the MEM program converges toward the most probable solution giving the correlation peaks. The deviation functions for each polarized decay component display a much more regular pattern: randomly dispersed around the zero value (not shown) and chi-square values close to the expected value of 1.0. As expected from the visual inspection of the experimental decay curve, the two-dimensional $\Gamma(\tau, \theta)$ maps of the rotational correlation times θ_i versus the excited-state lifetimes τ_i show a systematic association between the short-lived excited-state population and the fast rotating component (~150 ps) (Figure 5, panels A, B, and C). Conversely, the long-lived excited state population, characterizing the bound probe, is mainly associated with the Brownian rotational motion of the protein (Figure 5, panels B and C). A peak of weak amplitude associating the long lifetime and a fast rotation ($\theta \sim 150$ ps) is present (Figure 5, panel B). This suggests that the bound probe is slightly mobile in the binding site. A wobbling angle of rotation of ~20° is calculated from the $\Gamma(\tau, \theta)$ coefficients of the long lifetime component τ_3 using: $[\Gamma(\tau_2,\theta_3)/\Gamma(\tau_2,\theta_2) + \Gamma(\tau_2,\theta_3)] = (1/2)[\cos \omega_{max}(1 + \cos \omega_{max})]^2$, an expression similar to that used for monoexponential fluorescence decays (*40*). The bound fluorescent nucleotide becomes completely immobile in the ternary complex with CMP (Figure 5, panel C). CDP and dCMP, which did not display any large effects on the lifetime value, decrease the wobbling angle of rotation of the bound Ant-dADP by only ~50% (not shown).

Modeling of the $CMPK_{coli}$ Complexes with Ant-dADP. Crystallization of any binary ($CMPK_{coli}$/phosphate donor) or ternary ($CMPK_{coli}$/phosphate donor/phosphate acceptor) complexes remains unsuccessful despite continuous efforts. Therefore, we decided to model the $CMPK_{coli}$/Ant-dADP complex to locate the Ant-dADP in the phosphate donor binding site and to estimate its accessibility to the solvent. We compared our model to the structure of $UMPK_{dict}$ with substrates, which exhibits a closed conformation of the LID domain (*26*), to propose a likely conformation of the LID in the $CMPK_{coli}$/Ant-dADP and $CMPK_{coli}$/Ant-dADP/CMP complexes.

The superimposition of the crystal structures of $CMPK_{coli}$, $CMPK_{coli}$/CDP, and of $UMPK_{dict}$ complexed with substrates and AlF_3 suggests that the $CMPK_{coli}$ LID region is flexible (Figure 6, panel A). The α-helix 7 of the ligand-free $CMPK_{coli}$ superimposes well with the corresponding α-helix of $UMPK_{dict}$. It is rotated in the $CMPK_{coli}$/CDP structure with a maximum shift of 8 Å at position 164. The loop connecting α-helices 7 and 8 adopts an opened conformation in both $CMPK_{coli}$ and $CMPK_{coli}$/CDP structures. In $UMPK_{dict}$, this loop wraps around the ATP substrate, allowing the arginine residue R131 to interact with the β- and γ-phosphate groups of ATP (*41*). This suggests that the LID region of $CMPK_{coli}$ could move upon ATP (Ant-dADP) binding to reach a similar position as in $UMPK_{dict}$.

In the molecular model of the $CMPK_{coli}$/Ant-dADP complex constructed with $CMPK_{coli}$ without phosphate acceptor (1cke), the adenine ring of Ant-dADP is sandwiched between the R157 and the I209 side-chains (Figure 6, panel B). This structural feature characterizes all known UMP/CMP kinases (*26*, *32*, *42*, *43*). The equivalent residues are R127 and V178 in $UMPK_{dict}$ and R138 and V189 in $UMPK_{yeast}$. This structural motif, sandwiching the adenine ring between a basic residue and a hydrophobic side chain, is also present in other NMPKs. For instance, R119 and V202 occupy equivalent positions in $AMPK_{coli}$ (*44*). The corresponding residues in $TMPK_{coli}$ are R149 and L193 (*11*). By the way, recent site-directed mutagenesis experiments confirm the importance of the R149 residue for the binding of ATP and Ant-dADP to $TMPK_{coli}$ (unpublished results).

The β-phosphate of the fluorescent nucleotide is bound to the P-loop (Figure 6, panel B), where it undergoes

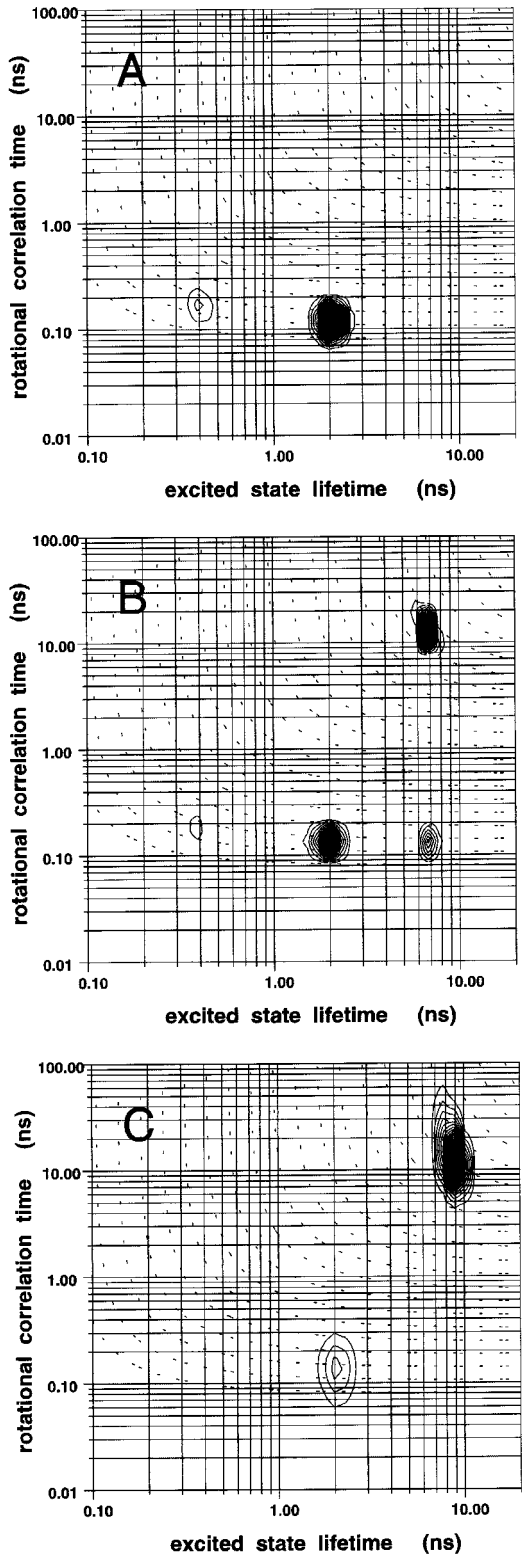

FIGURE 5: Two-dimensional $\Gamma(\tau, \theta)$ plots resulting from the MEM analysis of the polarized fluorescence decays of Ant-dADP. (A) Ant-dADP (3.8 μM) in water; (B) Ant-dADP (3.8 μM) in the presence of $CMPK_{coli}$ (10.8 μM) without CMP; (C) Ant-dADP (3.8 μM) in the presence of $CMPK_{coli}$ (10.8 μM) with 1 mM CMP. The fit was performed on the polarized fluorescence intensity decays $I_{vv}(t)$ and $I_{vh}(t)$ using their classical expressions: $I_{vv}(t) = (1/3)\int_0^\infty \int_0^\infty \Gamma(\tau, \theta) e^{-t/\tau}(1 + 2Ae^{-t/\theta}) d\tau d\theta$ and $I_{vh}(t) = (1/3)\int_0^\infty \int_0^\infty \Gamma(\tau, \theta) e^{-t/\tau}(1 - Ae^{-t/\theta}) d\tau d\theta$. $\Gamma(\tau, \theta)$ is the relative proportion of emittor with lifetime τ and correlation time θ, and A is the intrinsic anisotropy whose value is 0.34 as measured in vitrified glycerol at -80 °C. Excitation wavelength: 340 nm; emission wavelength: 410 nm.

interactions with the main chain nitrogens of residues 15 to 18 and with the ϵNH2 of Lys18. The anthraniloyl ring encounters residues 157 to 164 of α-helix 7. It points toward the entrance to the active site cavity. The CO and NH_2 groups are maintained in the gauche−gauche conformation as observed for the 3′-O-anthraniloyladenosine either in the crystals or in solution (*45*). Nevertheless, it undergoes contacts with few side chains, in particular L160 and Q161. The aromatic ring is exposed to the solvent (Figure 6, panel B). Calculation of the accessibility of the van der Waals surface of the anthraniloyl ring to a spherical probe (radius 1.4 Å) shows a relative solvent-accessible surface of 33% in the $CMPK_{coli}$/Ant-dADP complex. It increases to 45% in the $CMPK_{coli}$/CDP/Ant-dADP complex. For such an accessibility, the bimolecular quenching constant value for acrylamide should be of the order of $\sim 10^9$ M^{-1} s^{-1}, 5−6 times larger than the value we observed experimentally. To protect the anthraniloyl moiety from the solvent, a conformational change of the LID region likely occurs upon binding of the ATP analogue.

This ATP-induced conformational change of this region could explain the observed protection by ATP of $CMPK_{coli}$ against proteolytic cleavage by trypsin at position R158 (*4*). In this movement, this arginine residue could move near the phosphate groups in the complex with ATP, in a similar position as R131 in the structure of the $UMPK_{dict}$/ADP/CMP/AlF_3 complex (*41*).

DISCUSSION

We show in this work that Ant-dADP is a powerful tool allowing, due to its fluorescence properties, one to measure the dynamics of the ATP binding site of $CMPK_{coli}$ as well as its accessibility to the aqueous solvent. Thus we obtained the first set of experimental data about the expected changes induced by the phosphate donor on the structure and dynamics of the ATP binding site of this protein. The time-resolved fluorescence intensity measurement allows an easy separation of the excited-state lifetimes specific of the free and of the protein-bound Ant-dADP, which are both present owing to its relatively high K_d values (in the micromolar range) even in the presence of CMP. Then, the accessibility to the solvent of Ant-dADP can be specifically monitored using the quenching technique by acrylamide, a water-soluble reactant. The fluorescence anisotropy decays moreover evaluate separately the rotational parameters of both the free and the protein-bound Ant-dADP, and MEM analysis is able to describe the specific associations between lifetimes and correlation times. In these conditions, we are thus able to measure the fast internal motion of the bound probe and the Brownian motions of both the protein and the free probe.

Binding to $CMPK_{coli}$ strongly affects the spectroscopic characteristics of Ant-dADP. The excited-state lifetime displays a much larger value in the protein-bound state than in water, an observation also reported in other nucleotide binding proteins (*13*, *14*, *46*−*48*). The absorption and the excitation spectra of the bound Ant-dADP shift to longer wavelengths with respect to the spectra in water. Less protic solvents than water and to a larger extend aprotic polar solvents, display similar effects. The first excited state energy level is lower in organic polar solvents and its lifetime is longer, like in the protein-bound state. This bathochromic effect could be due to the existence of an additional

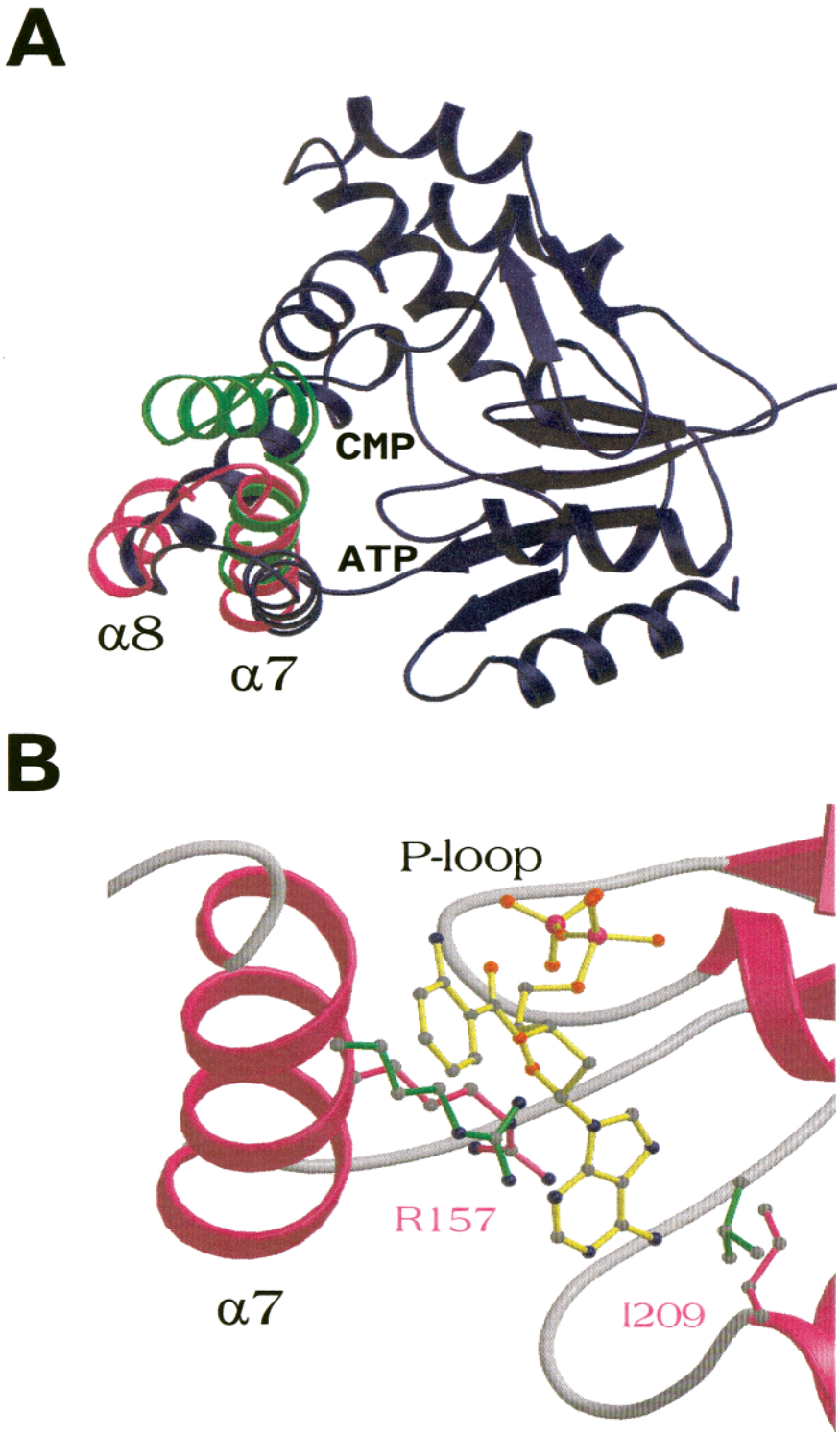

FIGURE 6: Conformational change of the LID domain and binding of Ant-dADP. (A) Backbone superimposition of ligand-free $CMPK_{coli}$ (PDB code 1cke, magenta), $CMPK_{coli}$/CDP (2cmk, blue), and $UMPK_{dict}$/ADP/CMP/AlF3 complex (3ukd, green), using only the core of the five-stranded β-sheet: helix α7 from ligand-free $CMPK_{coli}$ superimposes well to the corresponding helix of $UMPK_{dict}$. For $CMPK_{coli}$/CDP the whole structure is shown, and for the two other structures only the region from α7 to α8, which includes the LID, is shown. The phosphate acceptor and donor sites are labeled CMP and ATP, respectively. (B) Model of the $CMPK_{coli}$ complex with Ant-dADP (ball-and-stick, yellow sticks). Same orientation as in panel A, enlarged view. Side chains of residues sandwiching the adenine ring are emphasized through ball-and-stick representation: R157 and I209 from $CMPK_{coli}$ (magenta, labeled), and the two equivalent residues R127 and V178 (green) from $UMPK_{dict}$. Figure drawn using MOLSCRIPT (*59*, *60*).

resonance in the sixth-member ring possibly formed with the CO and the NH_2 groups on the benzene ring (*49*). This configuration may be favored by the major gauche−gauche conformation of these CO and NH_2 groups observed either in water solution or in the crystal of Ant-adenosine (*45*). This might facilitate the formation of an intramolecular H-bond, which could be in competition with the aqueous solvent. Quenching of the aqueous solvent by a mechanism involving a proton transfer is likely according to the observed isotopic effect of D_2O (*36*).

When Ant-dADP is bound to $CMPK_{coli}$, it is therefore shielded from the aqueous solvent either in the absence or

presence of CMP. This is in agreement with the weak quenching of the protein-bound Ant-dADP fluorescence by the water-soluble quencher acrylamide. A good agreement between accessibility of the anthraniloyl ring calculated from the three-dimensional structure and acrylamide quenching efficiency has been observed in other cases such as in the myosin motor domain of *Dictyostelium discoideum* (*46*).

Modeling of the $CMPK_{coli}$/Ant-dADP complex suggests that the anthraniloyl moiety should be solvent-accessible if no structural change was occurring in the LID domain. An ATP-induced conformational change of the LID, screening the nucleotide phosphate donor from the solvent, is therefore likely and could account for the spectroscopic data of Ant-dADP bound to $CMPK_{coli}$. In this respect, specific ATP-driven changes of secondary structure of $CMPK_{coli}$ and $CMPK_{subtilis}$ were observed by infrared measurements (*50*), although it was not possible to ascribe these changes to specific protein regions such as the LID or the NMP binding site or both.

This conformational change of the LID domain was directly observed in the crystal structure of only a few other nucleotide kinases such as AMPKs (*9*, *51*, *52*) and more recently like TMPKs (*53*, *54*), where the LID adopts a closed conformation in the complexes of these proteins with ATP analogues. In the case of AMPK, ATP binding closes the LID domain but to a lesser extent than in ternary complexes where the NMP binding site is occupied (*51*). The phosphate acceptor therefore provokes an additional conformational change, which has been also detected by time-resolved fluorescence energy transfer measurements (*55*, *56*). Significant changes in the protein mobility have been also suggested by the temperature B-factor values both in the LID and the NMP_{bind} regions between the free and the bound states of the AMPK protein (*10*).

CMP induces similarly a further change of the LID in the $CMPK_{coli}$/Ant-dADP complex, which suppresses the fast mobility of the ATP fluorescent analogue and tightly locks the catalytic site. The crystallographic data show that binding of CDP (or CMP or dCMP) leads to a closed conformation of the NMP_{bind} region and to a more opened conformation of the LID when the ATP site is unoccupied. The CMP-induced opening of the LID would favor ATP or ATP analogues to bind more efficiently to the $CMPK_{coli}$/CMP binary complex as previously observed (*4*). The present fluorescence data suggest that the binding of ATP to $CMPK_{coli}$ leads to a closure of the LID. The further rigidification by CMP would prevent the escape of ATP from the ternary complex during the phosphorylation process. The minor rigidification induced by CDP (as compared to CMP) would lead to an easier removal of ADP.

CONCLUSIONS

Ant-dADP, used as a reporter of the dynamic state of the ATP binding site of $CMPK_{coli}$, suggests the existence of a conformational change of the LID region provoked by the binding of the phosphate donor. This region probably wraps tightly around ATP and leads to its complete inaccessibility to the solvent, even in the absence of CMP. Moreover, the phosphate acceptor CMP provokes a complete immobilization of the ATP fluorescent analogue. The product CDP exhibits a weaker effect. Such substrate-induced fit leading to a protection of the active site from the aqueous solvent is the mechanism by which kinases avoid hydrolytic activity (*6*, *57*). These observations, together with the increase of the affinity of the phosphate donor analogues induced by CMP (*4*) suggest that the enzymatic reaction of CDP production proceeds by a mechanism in which the ternary complex $CMPK_{coli}$/CMP/ATP is formed sequentially by first binding of CMP followed by ATP.

ACKNOWLEDGMENT

The technical staff of LURE is acknowledged for running the synchrotron machine during the beam sessions. We thank Robert Sarfati for the synthesis of Ant-dADP.

REFERENCES

1. Anderson, E. P. (1973) in *The Enzymes* (Boyer, P. D., Ed.) pp 49−96, Academic Press, New York.
2. Neuhard, J., and Nygaard, P. (1987) in *Escherichia coli and Salmonella typhimurium: Cellular and Molecular Biology* (Neidhardt, F. C., Ingraham, J. L., Low, K. B., Magasanik, B., Schaechter, M., and Ulbarger, H. E., Eds.) pp 445−473, American Society for Microbiology, Washington, D. C.
3. Serina, L., Blondin, C., Krin, E., Sismeiro, O., Danchin, A., Sakamoto, H., Gilles, A. M., and Bârzu, O. (1995) *Biochemistry 34*, 5066−5074.
4. Bucurenci, N., Sakamoto, H., Briozzo, P., Palibroda, N., Serina, L., Sarfati, R. S., Labesse, G., Briand, G., Danchin, A., Barzu, O., and Gilles, A. M. (1996) *J. Biol. Chem. 271*, 2856−2862.
5. Briozzo, P., Golinelli-Pimpaneau, B., Gilles, A. M., Gaucher, J. F., Burlacu-Miron, S., Sakamoto, H., Janin, J., and Bârzu, O. (1998) *Structure 6*, 1517−1527.
6. Yan, H., and Tsai, M. D. (1999) *Adv. Enzymol. Relat. Areas Mol. Biol. 73*, 103−134.
7. Schulz, G. E., Müller, C. W., and Diederichs, K. (1990) *J. Mol. Biol. 213*, 627−630.
8. Berry, M. B., Meador, B., Bilderback, T., Liang, P., Glaser, M., and Phillips, G. N., Jr. (1994) *Proteins 19*, 183−198.
9. Vonrhein, C., Schlauderer, G. J., and Schulz, G. E. (1995) *Structure 3*, 483−490.
10. Müller, C. W., Schlauderer, G. J., Reinstein, J., and Schulz, G. E. (1996) *Structure 4*, 147−156.
11. Lavie, A., Ostermann, N., Brundiers, R., Goody, R., Reinstein, J., Konrad, M., and Schlichting, I. (1998) *Proc. Natl. Acad. Sci. U.S.A. 95*, 14045−14050.
12. Hiratsuka, T. (1982) *J. Biol. Chem. 257*, 13354−13358.
13. Jameson, D., and Eccleston, J. F. (1997) *Methods Enzymol. 278*, 363−390.
14. Hazlett, T. L., Moore, K. J. M., Lowe, P. N., Jameson, D., and Eccleston, J. F. (1993) *Biochemistry 32*, 13575−13583.
15. Sarfati, R. S., Kansal, V. K., Munier, H., Glaser, P., Gilles, A. M., Labruyère, E., Mock, M., Danchin, A., and Bârzu, O. (1990) *J. Biol. Chem. 265*, 18902−18906.
16. Blondin, C., Serina, L., Wiesmüller, L., Gilles, A. M., and Bârzu, O. (1994) *Anal. Biochem. 220*, 219−221.
17. Vincent, M., Gallay, J., and Demchenko, A. D. (1995) *J. Phys. Chem. 99*, 14931−14941.
18. Brochon, J.-C. (1994) *Methods Enzymol. 240*, 262−311.
19. Livesey, A. K., and Brochon, J.-C. (1987) *Biophys. J. 52*, 693−706.
20. Vincent, M., and Gallay, J. (1991) *Eur. Biophys. J. 20*, 183−91.
21. Vincent, M., Brochon, J. C., Merola, F., Jordi, W., and Gallay, J. (1988) *Biochemistry 27*, 8752−8761.
22. Gentin, M., Vincent, M., Brochon, J. C., Livesey, A. K., Cittanova, N., and Gallay, J. (1990) *Biochemistry 29*, 10405−10412.
23. Rouvière, N., Vincent, M., Craescu, C. T., and Gallay, J. (1997) *Biochemistry 36*, 7339−7352.
24. Sopkova, J., Vincent, M., Takahashi, M., Lewit-Bentley, A., and Gallay, J. (1998) *Biochemistry 37*, 11962−11970.

25. Sopkova, J., Vincent, M., Takahashi, M., Lewit-Bentley, A., and Gallay, J. (1999) *Biochemistry 38*, 5447−5458.
26. Schlichting, I., and Reinstein, J. (1997) *Biochemistry 36*, 9290−9296.
27. Li de la Sierra, I., Quillien, L., Flecker, P., Gueguen, J., and Brunie, S. (1999) *J. Mol. Biol. 285*, 1195−1207.
28. Jones, T. A., Zou, J. Y., Cowan, S. W., and Kjeldgaard, M. (1991) *Acta Crystallogr. A47*, 110−119.
29. Dreusicke, D., Karplus, P. A., and Schultz, G. E. (1992) *J. Mol. Biol. 199*, 359−371.
30. Diederichs, K., and Schulz, G. E. (1991) *J. Mol. Biol. 217*, 541−549.
31. Stehle, T., and Schultz, G. E. (1992) *J. Mol. Biol. 224*, 1127−1141.
32. Müller-Dieckmann, H. J., and Schulz, G. E. (1994) *J. Mol. Biol. 236*, 361−367.
33. Vonrhein, C., Bönisch, H., Schäfer, G., and Schulz, G. E. (1998) *J. Mol. Biol. 282*, 167−179.
34. Brünger, A., Kuriyan, J., and Karplus, M. (1987) *Science 235*, 458−460.
35. Scheidig, A. J., Franken, S. M., Corrie, J. E., Reid, G. P., Wittinghofer, A., Pai, E. F., and Goody, R. S. (1995) *J. Mol. Biol. 253*, 132−150.
36. Stryer, L. (1966) *J. Am. Chem. Soc. 88*, 5708−5712.
37. Eftink, M. R., and Ghiron, C. A. (1981) *Anal. Biochem. 114*, 199−227.
38. Eftink, M. R. (1991) in *Topics in Fluorescence Spectroscopy* (Lakowicz, J. R., Ed.) pp 53−126, Plenum Press, New York and London.
39. Johnson, D. A., and Yguerabide, J. (1985) *Biophys. J. 48*, 949−955.
40. Kawato, S., Kinosita, K. J., and Ikegami, A. (1977) *Biochemistry 16*, 2319−2324.
41. Schlichting, I., and Reinstein, J. (1999) *Nat. Struct. Biol. 6*, 721−723.
42. Muller-Dieckmann, H. J., and Schulz, G. E. (1995) *J. Mol. Biol. 246*, 522−530.
43. Scheffzek, K., Kliche, W., Wiesmüller, L., and Reinstein, J. (1996) *Biochemistry 35*, 9716−9727.
44. Müller, C. W., and Schulz, G. E. (1992) *J. Mol. Biol. 224*, 159−177.
45. Nawrot, B., Milius, W., Ejchart, A., Limmer, S., and Sprinzl, M. (1997) *Nucl. Acids Res. 25*, 948−954.
46. Bauer, C. B., Kuhlman, P. A., Bagshaw, C. R., and Rayment, I. (1997) *J. Mol. Biol. 274*, 394−407.
47. Bujalowski, W., and Klonowska, M. M. (1994) *Biochemistry 33*, 4682−4694.
48. Mocz, G., Helms, M. K., Jameson, D. M., and Gibbons, I. R. (1998) *Biochemistry 37*, 9862−6869.
49. Clar, E. (1964) *Polycyclic Hydrocarbons*, Springer-Verlag, Berlin.
50. Schultz, C. P., Ylisastigui-Pons, L., Serina, L., Sakamoto, H., Mantsch, H. H., Neuhard, J., Bârzu, O., and Gilles, A. M. (1997) *Arch. Biochem. Biophys. 340*, 144−153.
51. Schlauderer, G. J., Proba, K., and Schulz, G. E. (1996) *J. Mol. Biol. 256*, 223−227.
52. Schlauderer, G. J., and Schulz, G. E. (1996) *Protein Sci. 5*, 434−441.
53. Lavie, A., Vetter, I. R., Konrad, M., Goody, R. S., Reinstein, J., and Schlichting, I. (1997) *Nat. Struct. Biol. 4*, 601−604.
54. Lavie, A., Schlichting, I., Vetter, I. R., Konrad, M., Reinstein, J., and Goody, R. S. (1997) *Nat. Med. 3*, 922−924.
55. Sinev, M. A., Sineva, E. V., Ittah, V., and Haas, E. (1996) *FEBS Lett. 397*, 273−276.
56. Sinev, M. A., Sineva, E. V., Ittah, V., and Haas, E. (1996) *Biochemistry 35*, 6425−6437.
57. Koshland, D. E. J. (1994) *Angew. Chem., Int. Ed. Engl. 33*, 2375−2378.
58. Wahl, P. (1979) *Biophys. Chem. 10*, 91−104.
59. Kraulis, P. J. (1991) *J. Appl. Crystallogr. 24*, 946−950.
60. Merrit, E. A., and Murphy, M. E. (1994) *Acta Crystallogr. D 50*, 869−873.

BI0015360